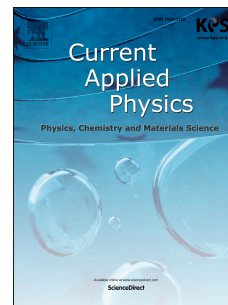


# Accepted Manuscript

Potentiostatic and Galvanostatic Electrodeposition of Manganese Oxide for Supercapacitor Application: A Comparison Study

Gomaa A.M. Ali, Mashitah M. Yusoff, Yun Hau Ng, Hong Ngee Lim, Chong Kwok Feng



PII: S1567-1739(15)30010-9

DOI: [10.1016/j.cap.2015.06.022](https://doi.org/10.1016/j.cap.2015.06.022)

Reference: CAP 4006

To appear in: *Current Applied Physics*

Received Date: 5 February 2015

Revised Date: 18 May 2015

Accepted Date: 25 June 2015

Please cite this article as: G.A.M. Ali, M.M. Yusoff, Y.H. Ng, H.N. Lim, C.K. Feng, Potentiostatic and Galvanostatic Electrodeposition of Manganese Oxide for Supercapacitor Application: A Comparison Study, *Current Applied Physics* (2015), doi: 10.1016/j.cap.2015.06.022.

This is a PDF file of an unedited manuscript that has been accepted for publication. As a service to our customers we are providing this early version of the manuscript. The manuscript will undergo copyediting, typesetting, and review of the resulting proof before it is published in its final form. Please note that during the production process errors may be discovered which could affect the content, and all legal disclaimers that apply to the journal pertain.

# Potentiostatic and Galvanostatic Electrodeposition of Manganese Oxide for Supercapacitor Application: A Comparison Study

Gomaa A. M. Ali <sup>a,b</sup>, Mashitah M. Yusoff <sup>a</sup>, Yun Hau Ng <sup>c</sup>, Hong Ngee Lim <sup>d</sup>, Chong

Kwok Feng <sup>a,\*</sup>

<sup>a</sup> Faculty of Industrial Sciences & Technology, Universiti Malaysia Pahang, 26300 Kuantan, Malaysia

<sup>b</sup> Chemistry Department, Faculty of Science, Al-Azhar University, Assiut, 71524, Egypt

<sup>c</sup> Particles and Catalysis Research Group, School of Chemical Engineering, The University of New South Wales, Sydney NSW 2052, Australia

<sup>d</sup> Department of Chemistry, Faculty of Science, Universiti Putra Malaysia, 43400 UPM Serdang, Selangor, Malaysia

\*Author for correspondence: (email: [ckfeng@ump.edu.my](mailto:ckfeng@ump.edu.my); Tel.: +609 5492403; Fax: +609 5492766)

## Abstract

The structural and electrochemical properties of manganese oxide ( $\text{MnO}_2$ ) electrodeposited by potentiostatic and galvanostatic conditions are studied. X-ray diffraction analyses confirm identical  $\text{MnO}_2$  phase (ramsdellite) are deposited under potentiostatic and galvanostatic conditions. Under comparable current density during electrodeposition,  $\text{MnO}_2$  deposited by galvanostatic condition shows smaller crystallite size, less compact layered structure, higher surface area and wider band gap, in comparison to the potentiostatic

deposition. The MnO<sub>2</sub> morphology difference under different electrodeposition conditions contributes to different capacitive behaviors. The lower compactness of MnO<sub>2</sub> deposited galvanostatically renders facile ions diffusion, leading to higher specific capacitance with low equivalent series resistance. The findings suggest galvanostatic electrodeposition is suitable to produce MnO<sub>2</sub> nanostructure for supercapacitor application.

**Keywords:** Potentiostatic, Galvanostatic, Electrodeposition, Supercapacitors, Manganese oxide

## 1. Introduction

In recent years, MnO<sub>2</sub> is attracting attention for supercapacitor application, mainly due to the high abundancy of manganese [1] that contributes to low material cost as compared to the expensive ruthenium metal. Pang et al. reported high specific capacitance (700 F g<sup>-1</sup>) for MnO<sub>2</sub> thin films in year 2000 and their findings sparked strong interest among energy research community for its application in supercapacitor electrode [2, 3]. Such high capacitance value is attributed to the ions insertion/desertion within MnO<sub>2</sub> structure and it depends crucially on the particle size, surface area and porosity. Since then, in achieving optimized condition for the aforementioned properties, MnO<sub>2</sub> with different morphologies were developed, such as nanoflakes [4], nanorods [5], nanowires [6], nanopetals [7] and nanosheets [8]. In this context, the synthesis route plays a vital role in determining its morphology. The most common synthesis route for MnO<sub>2</sub> is chemical coprecipitation method [9, 10] that involves dissolved Mn<sup>4+</sup> precursor. However, the instability of Mn<sup>4+</sup> precursor in

the aqueous solution as well as the contact resistance between synthesized  $\text{MnO}_2$  and current collectors hinders its common usage in electrochemical applications [11, 12]. Apart from chemical coprecipitation method, electrochemical deposition was proven to be an effective method to prepare  $\text{MnO}_2$  nanostructures [5, 13, 14]. There are two approaches for electrochemical deposition of  $\text{MnO}_2$ , namely anodic oxidation and cathodic reduction. Cationic  $\text{Mn}^{2+}$  precursor is commonly used in anodic oxidation while anionic  $\text{MnO}_4^-$  ( $\text{Mn}^{7+}$ ) is used in cathodic reduction. In comparison, cathodic reduction offers more versatility as various metals could be co-deposited during the deposition process and the oxidation of the metallic substrate during anodic deposition could also be avoided [6, 15, 16]. The cathodic reduction of  $\text{MnO}_4^-$  in neutral aqueous solutions can be represented by the following reaction [17]:



The kinetic pathway of reducing  $\text{Mn}^{7+}$  to  $\text{Mn}^{4+}$  is an important factor in determining  $\text{MnO}_2$  microstructure and it could be manipulated by potential and current during electrodeposition process [6, 7, 17]. In this context, galvanostatic and potentiostatic techniques are widely employed to electrochemically produce  $\text{MnO}_2$  nanostructures [6, 11, 13, 18]. Suhasini reported the comparison study between  $\text{MnO}_2$  films electrodeposited by potentiostatic and galvanostatic techniques, and demonstrated the galvanostatic technique could produce  $\text{MnO}_2$  film with higher specific capacitance [19]. However, the reported study only referred to the anodic deposition of  $\text{MnO}_2$  and there are limited studies report on the cathodic deposition of  $\text{MnO}_2$ . Herein, we report the comparative findings on the structural

and electrochemical properties of MnO<sub>2</sub> deposited cathodically under potentiostatic and galvanostatic conditions.

## 2. Experimental section

MnO<sub>2</sub> was electrodeposited cathodically from 0.5 M KMnO<sub>4</sub> solution by potentiostatic [denoted as MnO<sub>2</sub>(PS) hereafter] and galvanostatic [denoted as MnO<sub>2</sub>(GS) hereafter] conditions by applying 10 V and 0.165 A cm<sup>-2</sup> for 30 min at room temperature, respectively. The stainless steel substrate (1x2 cm<sup>-2</sup>) was first etched in hydrochloric acid (0.1 M) and in acetone for 1 hour, then washed and dried. Two pre-treated stainless steel plates were used as the electrodes. The distance between two electrodes was kept constant at 20 mm throughout the electrodeposition process. For both electrodeposition techniques, black films were obtained on the cathode and the mass was recorded after drying.

Phase identification of the films was carried out using a PHILLIPS PW1700 diffractometer equipped with an automatic divergent slit. Diffraction patterns were obtained using Cu-K<sub>α</sub> radiation ( $\lambda = 0.15418$  nm) and a graphite monochromator in the  $2\theta$  range from 5° to 80°. Sample morphology was investigated using a JEOL JSM-7800F field emission scanning electron microscope. The surface area of the samples were measured by NOVA 3200 surface area analyser. The optical absorption spectra were measured at the wavelength range from 200 to 900 nm at room temperature using a THERMO SCIENTIFIC UV-Vis spectrophotometer. The electrochemical measurements were conducted in 1 M Na<sub>2</sub>SO<sub>4</sub> with three-electrode system consisting MnO<sub>2</sub> coated stainless steel plate as working electrode, Ag/AgCl as reference electrode and Pt wire as counter electrode. Cyclic voltammetry (CV) tests and galvanostatic charge-discharge tests were conducted in the potential range between 0 and 1 V. Impedance data were collected from 100 kHz to 0.01 Hz, at open circuit potential

with an AC amplitude signal of 10 mV. All electrochemical data were collected using AUTOLAB PGSTAT M101 potentiostat/galvanostat equipped with frequency response analyzer.

### 3. Results and discussion

Figure 1 shows the XRD patterns of MnO<sub>2</sub>(PS) and MnO<sub>2</sub>(GS). Both XRD patterns confirm the black films on the stainless steel electrodes as the ramsdellite phase MnO<sub>2</sub> (ICCD 96 900 1168). For both XRD patterns, two XRD peaks at 44.5° and 65.8° could be attributed to the stainless steel ((ICCD 00 087 7222)). Crystallite size calculation by the Scherrer formula shows that the MnO<sub>2</sub>(PS) has bigger crystallite size (23 nm) as compared to that obtained on MnO<sub>2</sub>(GS) (18 nm). The crystallite size of MnO<sub>2</sub> is known to affect the ions (de)intercalation rate and therefore regulating the performance of a supercapacitor [20].

The sample morphology was investigated by FESEM and the representative images are shown in Figure 2. Both electrodeposition conditions produce similar layered structure of MnO<sub>2</sub> that only differs in the nanosheets compactness. MnO<sub>2</sub>(GS) shows lower nanosheets compactness and the nanosheets are greatly separated from each other, in comparison to the MnO<sub>2</sub>(PS). The difference in the nanosheets compactness and morphology under different deposition conditions could be explained from the potential response (left y axis for galvanostatic) and current response (right y axis for potentiostatic) during electrodeposition process (Figure 3). In this study, 10 V was carefully selected for the potentiostatic deposition as it generated current density in the range that was comparable to the current density applied (0.165 A cm<sup>-2</sup>) in the galvanostatic deposition. The total charge passing through the electrode was calculated for both deposition conditions and they show almost identical values (293 C cm<sup>-2</sup> for potentiostatic; 297 C cm<sup>-2</sup> for galvanostatic).

Since total consumed charge values are almost identical for both deposition processes, the difference in MnO<sub>2</sub> morphology could be attributed to the potential difference during electrodeposition process. For galvanostatic deposition for MnO<sub>2</sub>(GS), it could be observed that the potential gradually decreases with time, due to the enhanced friction effect resulting from MnO<sub>2</sub> formation on the cathode and the interaction of ions moving in cathodic direction with the ions electromigrating in anodic direction. The potential drop decreases the diffusion rate of MnO<sub>4</sub><sup>-</sup> to the cathode surface and allows lower deposition rate, thus producing MnO<sub>2</sub>(GS) layered structure with less compact nanosheets, as shown in the FESEM image. For potentiostatic deposition for MnO<sub>2</sub>(PS), the potential is maintained throughout the deposition process and MnO<sub>2</sub> structure is formed rapidly, producing layered structure with compact nanosheets. For both deposition techniques, H<sub>2</sub> evolution occurs and pushes the Mn species to the vacant areas of the substrate which is free from the H<sub>2</sub> bubbles, leading to the formation of layered structure. Similar findings are obtained elsewhere for MnO<sub>2</sub> and other nanomaterials [21, 22].

Figure 4 shows the N<sub>2</sub> adsorption–desorption isotherms of MnO<sub>2</sub>(GS) and MnO<sub>2</sub>(PS), with the pore size distribution as inset. The specific surface areas are found to be 63.5 and 36.6 m<sup>2</sup> g<sup>-1</sup> for MnO<sub>2</sub>(GS) and MnO<sub>2</sub>(PS), respectively. Pore size distribution curves show the pore size ranges from 2 to 70 nm (two narrow peaks around 3 and 20 nm) and from 2 to 20 nm for MnO<sub>2</sub>(GS) and MnO<sub>2</sub>(PS), respectively. The lower nanosheets compactness of MnO<sub>2</sub>(GS) contributes to higher surface area and wider range of mesoporosity. The mesopores play an important role in enhancing the adsorption of ions during the electrochemical measurements.

The crystallite size and morphology affect the electronic and electrochemical properties of a nanostructure. The electronic properties of MnO<sub>2</sub>(PS) and MnO<sub>2</sub>(GS) were investigated by band gap studies. MnO<sub>2</sub> exhibits broad absorption band at ca. 400 nm, which is the characteristic of the excitation from O<sub>2p</sub> to Mn<sub>3d</sub> [23]. The absorption band gap ( $E_g$ ) was obtained from the following equation [24]:

$$(\alpha hv)^n = \beta(hv - E_g) \quad (2)$$

where,  $hv$  is the photon energy,  $\beta$  is a constant relative to the material,  $E_g$  is the energy band gap,  $\alpha$  is the absorption coefficient and the exponent  $n$  takes different values depending on electronic transition types in the  $K$  space (2 for direct allowed, 2/3 for direct forbidden, 1/2 for indirect allowed and 1/3 for indirect forbidden transition). The absorption coefficient ( $\alpha$ ) was calculated as reported elsewhere [24]. Extrapolation of the linear line to zero absorption coefficients gives the values of energy band gap as shown in Figure 5. The energy band gaps are found to be 1.85 and 1.95 eV for MnO<sub>2</sub>(PS) and MnO<sub>2</sub>(GS), respectively. The wider band gap for MnO<sub>2</sub>(GS) could be attributed to the smaller crystallite size of the nanostructure, as seen from the XRD analysis. Wider band gap indicates greater charge separation and higher carrier density will be generated under electrical field. The Mott–Schottky relationship predicts the interfacial capacitance (per unit surface area) increases with carrier density of the nanostructure [25]. Thus, it is noteworthy to investigate the capacitance of MnO<sub>2</sub> deposited under potentiostatic and galvanostatic conditions.

Figure 6(a) shows the CV curves for MnO<sub>2</sub>(PS) and MnO<sub>2</sub>(GS). The CV curve for MnO<sub>2</sub>(GS) shows larger rectangular loop with ideal symmetry which indicates better charge propagation within the nanostructure, as compared to the MnO<sub>2</sub>(PS). It could be associated with better nanosheets spacing and less compactness of the structure that facilitates ions

diffusion within the structure. The galvanostatic charge–discharge curves of MnO<sub>2</sub> deposited in two different approaches are displayed in Figure 6(b). Both curves are almost linear with neglected iR drop, suggesting the rapid current-voltage response of the MnO<sub>2</sub>. Furthermore, the symmetrical charge-discharge curves also indicate the good reversibility of MnO<sub>2</sub> deposited in two different approaches. The specific capacitance values were calculated from the slope of discharge curve using the equation reported elsewhere [26]. As suggested by the band gap results, MnO<sub>2</sub>(GS) with wider band gap shows higher specific capacitance (196 F g<sup>-1</sup> at 1 A g<sup>-1</sup>), in comparison to the MnO<sub>2</sub>(PS) (128 F g<sup>-1</sup> at 1 A g<sup>-1</sup>). MnO<sub>2</sub> deposited by both techniques show similar trend in which the specific capacitance values increase with lower current density, as shown in Figure 6(c). This trend is attributed to the slower ions diffusion at lower current density that contributes to higher ions adsorption. However, the specific capacitance values for MnO<sub>2</sub>(PS) decrease drastically at higher current density, which could be related to the high compactness of MnO<sub>2</sub>(PS) structure that limits the penetration of ions into the inner region due to fast potential change at high current density. These findings suggest MnO<sub>2</sub>(GS) is more suitable to be deployed as supercapacitor electrode, even at high current density load. The stability tests were conducted by continuous charge-discharge MnO<sub>2</sub> at 5 A g<sup>-1</sup> and the results are presented in Figure 6(d). After 5000 cycles of charge-discharge, MnO<sub>2</sub>(GS) shows higher stability with 88% of capacitance retention, as compared to the 75% for MnO<sub>2</sub>(PS). Moreover, the coulombic efficiency (Figure 6(d) inset) for MnO<sub>2</sub>(GS) was found to be higher than that obtained for MnO<sub>2</sub>(PS) after 5000 cycles charge-discharge. Such findings could be explained by the high compactness of MnO<sub>2</sub>(PS) structure that could easily be clogged up during long charge-discharge cycles.

Figure 7 shows the Nyquist plots for MnO<sub>2</sub>(GS) and MnO<sub>2</sub>(PS). MnO<sub>2</sub>(GS) shows shorter Warburg diffusion at low frequency, possibly due to the better nanosheets spacing and less compactness of the structure. Insets of Figure 7 show the zoomed impedance plots at high frequency region and the equivalent circuit fitting. The corresponding fitted data is tabulated in Table 1. The intercept at  $x$  axis represents the equivalent series resistance (ESR) which can be related to the conductivity of the material. It could be seen that the ESR for MnO<sub>2</sub>(GS) is 1.52  $\Omega$ , lower as compared to the 2.21  $\Omega$  for MnO<sub>2</sub>(PS). The lower ESR value could be attributed to the higher carrier density of the MnO<sub>2</sub>(GS). In addition, galvanostatic technique produces MnO<sub>2</sub>(GS) with lower charge transfer resistance than that obtained on MnO<sub>2</sub>(PS). The electroactive surface area was calculated from the impedance data, according to the formula reported elsewhere [4]. The electroactive surface area for MnO<sub>2</sub>(GS) was calculated to be 190 cm<sup>2</sup> g<sup>-1</sup>, that is about 2 folds higher than the 108 cm<sup>2</sup> g<sup>-1</sup> surface area for MnO<sub>2</sub>(PS), probably due to the less compactness of the nanosheets for MnO<sub>2</sub>(GS). The higher electroactive surface area explains the better capacitive behavior of MnO<sub>2</sub>(GS), as suggested by CV and charge-discharge data.

Table 1: Equivalent circuit fitting parameters for MnO<sub>2</sub>(GS) and MnO<sub>2</sub>(PS).

	$R_s$ ( $\Omega$ )	$R_{ct}$ ( $\Omega$ )	$C$ ( $mF$ )	$Q$ ( $mF$ )	$S_E$ ( $m^2 g^{-1}$ )	$W$ ( $\Omega$ )
<b>MnO<sub>2</sub>(GS)</b>	1.52	1.30	149.9	20.2	190	0.05
<b>MnO<sub>2</sub>(PS)</b>	2.21	1.91	85.1	10.2	108	0.09

#### 4. Conclusions

Comparison study for MnO<sub>2</sub>(GS) and MnO<sub>2</sub>(PS) shows the difference in terms of morphology, surface area, band energy and electrochemical properties. Galvanostatic technique could deposit MnO<sub>2</sub>(GS) in smaller crystallite size, layered structure with less compact nanosheets, higher surface area and wider band gap, as compared to the potentiostatic technique. Electrodeposited MnO<sub>2</sub> has been widely used in supercapacitor application and our findings show that MnO<sub>2</sub>(GS) is more suitable to be applied as supercapacitor electrode, due to the higher specific capacitance, lower ESR and higher electroactive surface area.

#### Acknowledgement

KF Chong and co-workers would like to acknowledge the funding from the Ministry of Education Malaysia in the form of MTUN-COE grant RDU121212 and RDU121213 and Ministry of Science, Technology and Innovation in the form of eScienceFund RDU140501.

#### References

- [1] D.Z.W. Tan, H. Cheng, S.T. Nguyen, H.M. Duong, Controlled synthesis of MnO<sub>2</sub>/CNT nanocomposites for supercapacitor applications, *Mater. Technol.* 29(2) (2014) 107-113.
- [2] S.-C. Pang, M.A. Anderson, T.W. Chapman, Novel electrode materials for thin-film ultracapacitors comparison of electrochemical properties of sol-gel-derived, *J. Electrochem. Soc.* 147(2) (2000) 444-450.
- [3] S.-C. Pang, M.A. Anderson, Novel electrode materials for electrochemical capacitors Part II. Material characterization of sol-gel-derived and electrodeposited manganese dioxide thin films, *J. Mater. Res.* 15(10) (2000) 2096-2106.

- [4] A.A. Radhiyah, M.I. Izwan, V. Baiju, C.K. Feng, I. Jamil, R. Jose, Doubling of electrochemical parameters via the pre-intercalation of  $\text{Na}^+$  in layered  $\text{MnO}_2$  nanoflakes compared to  $\alpha\text{-MnO}_2$  nanorods, *RSC Adv.* 5(13) (2015) 9667-9673.
- [5] T. Yousefi, A.N. Golikand, M. Hossein Mashhadizadeh, M. Aghazadeh, Facile synthesis of  $\alpha\text{-MnO}_2$  one-dimensional (1D) nanostructure and energy storage ability studies, *J. Solid State Chem.* 190 (2012) 202-207.
- [6] T. Yousefi, R. Davarkhah, A.N. Golikand, M.H. Mashhadizadeh, Synthesis, characterization, and supercapacitor studies of manganese (IV) oxide nanowires, *Mater. Sci. Semicond. Process.* 16(3) (2013) 868-876.
- [7] G. Yang, B. Wang, W. Guo, Z. Bu, C. Miao, T. Xue, H. Li, Liquid crystalline phase synthesis of nanoporous  $\text{MnO}_2$  thin film arrays as an electrode material for electrochemical capacitors, *Mater. Res. Bull.* 47(11) (2012) 3120-3123.
- [8] D. Yan, Z. Guo, G. Zhu, Z. Yu, H. Xu, A. Yu,  $\text{MnO}_2$  film with three-dimensional structure prepared by hydrothermal process for supercapacitor, *J. Power Sources* 199 (2012) 409-412.
- [9] R. Jiang, T. Huang, J. Liu, J. Zhuang, A. Yu, A novel method to prepare nanostructured manganese dioxide and its electrochemical properties as a supercapacitor electrode, *Electrochim. Acta* 54(11) (2009) 3047-3052.
- [10] X. Wang, Y. Zheng, Z. Xu, X. Wang, X. Chen, Amorphous  $\text{MnO}_2$  supported on carbon nanotubes as a superior catalyst for low temperature NO reduction with  $\text{NH}_3$ , *RSC Advances* 3(29) (2013) 11539-11542.
- [11] K.R. Prasad, N. Miura, Potentiodynamically deposited nanostructured manganese dioxide as electrode material for electrochemical redox supercapacitors, *J. Power Sources* 135(1-2) (2004) 354-360.
- [12] C. Xu, B. Li, H. Du, F. Kang, Y. Zeng, Electrochemical properties of nanosized hydrous manganese dioxide synthesized by a self-reacting microemulsion method, *J. Power Sources* 180(1) (2008) 664-670.
- [13] X. Hu, X. Lin, Z. Ling, Y. Li, X. Fu, Fabrication and characteristics of galvanostatic electrodeposited  $\text{MnO}_2$  on porous nickel from etched aluminium, *Electrochim. Acta* 138 (2014) 132-138.

- [14] G.A.M. Ali, L.L. Tan, R. Jose, M.M. Yusoff, K.F. Chong, Electrochemical performance studies of MnO<sub>2</sub> nanoflowers recovered from spent battery, *Mater. Res. Bull.* 60 (2014) 5-9.
- [15] J. Li, I. Zhitomirsky, Cathodic electrophoretic deposition of manganese dioxide films, *Colloids Surf., A* 348(1-3) (2009) 248-253.
- [16] J. Wei, M. Cheong, N. Nagarajan, I. Zhitomirsky, Cathodic electrodeposition of manganese oxides for electrochemical supercapacitors, *ECS Trans.* 3(37) (2007) 1-9.
- [17] G.M. Jacob, I. Zhitomirsky, Microstructure and properties of manganese dioxide films prepared by electrodeposition, *Appl. Surf. Sci.* 254(20) (2008) 6671-6676.
- [18] D. Das, P.K. Sen, K. Das, Mechanism of potentiostatic deposition of MnO<sub>2</sub> and electrochemical characteristics of the deposit in relation to carbohydrate oxidation, *Electrochim. Acta* 54(2) (2008) 289-295.
- [19] Suhasini, Effect of deposition method and the surfactant on high capacitance of electrochemically deposited MnO<sub>2</sub> on stainless steel substrate, *J. Electroanal. Chem.* 690 (2013) 13-18.
- [20] L. Feng, Z. Xuan, H. Zhao, Y. Bai, J. Guo, C.W. Su, X. Chen, MnO<sub>2</sub> prepared by hydrothermal method and electrochemical performance as anode for lithium-ion battery, *Nanoscale research letters* 9(1) (2014) 290-298.
- [21] G.R. Li, Z.P. Feng, Y.N. Ou, D. Wu, R. Fu, Y.X. Tong, Mesoporous MnO<sub>2</sub>/carbon aerogel composites as promising electrode materials for high-performance supercapacitors, *Langmuir* 26(4) (2010) 2209-2213.
- [22] X.H. Xia, J.P. Tu, Y.Q. Zhang, Y.J. Mai, X.L. Wang, C.D. Gu, X.B. Zhao, Three-dimensional porous nano-Ni/Co(OH)<sub>2</sub> nanoflake composite film: A pseudocapacitive material with superior performance, *J. Phys. Chem. C* 115(45) (2011) 22662-22668.
- [23] B.A. Pinaud, Z. Chen, D.N. Abram, T.F. Jaramillo, Thin films of sodium birnessite-type MnO<sub>2</sub>: Optical properties, electronic band structure, and solar photoelectrochemistry, *J. Phys. Chem. C* 115(23) (2011) 11830-11838.
- [24] G.A.M. Ali, O.A. Fouad, S.A. Makhlof, Structural, optical and electrical properties of sol-gel prepared mesoporous Co<sub>3</sub>O<sub>4</sub>/SiO<sub>2</sub> nanocomposites, *J. Alloys Compd.* 579 (2013) 606-611.

- [25] M. Jayalakshmi, M.M. Rao, K.-B. Kim, Effect of particle size on the electrochemical capacitance of  $\alpha$ -Ni(OH)<sub>2</sub> in alkali solutions, *Int. J. Electrochem. Sci.* 1 (2006) 324-333.
- [26] G.A.M. Ali, O.A. Fouad, S.A. Makhlof, M.M. Yusoff, K.F. Chong, Co<sub>3</sub>O<sub>4</sub>/SiO<sub>2</sub> nanocomposites for supercapacitor application, *J. Solid State Electrochem.* 18(9) (2014) 2505-2512.

ACCEPTED MANUSCRIPT

**Figure captions**

- Figure 1** XRD spectra for MnO<sub>2</sub>(PS) and MnO<sub>2</sub>(GS).
- Figure 2** Representative FESEM images at the same magnification for (a) MnO<sub>2</sub>(PS) and (b) MnO<sub>2</sub>(GS).
- Figure 3** Potential response (left y axis for galvanostatic) and current response (right y axis for potentiostatic) during electrodeposition process.
- Figure 4** N<sub>2</sub> adsorption–desorption isotherms of MnO<sub>2</sub>(PS) and MnO<sub>2</sub>(GS). The inset shows the pore size distributions.
- Figure 5** Direct transition  $(ah\nu)^2$  versus  $h\nu$  curves for (a) MnO<sub>2</sub>(PS) and (b) MnO<sub>2</sub>(GS).
- Figure 6** Electrochemical studies of MnO<sub>2</sub>(PS) and MnO<sub>2</sub>(GS) in 1 M Na<sub>2</sub>SO<sub>4</sub>. (a) CV curves for at 25 mV s<sup>-1</sup>; (b) Galvanostatic charge–discharge curves at 1 A g<sup>-1</sup>; (c) the variation of specific capacitance values as a function of current density and (d) cycling stability tests at 5 A g<sup>-1</sup>, the inset shows the coulombic efficiency.
- Figure 7** Nyquist plots for MnO<sub>2</sub>(PS) and MnO<sub>2</sub>(GS), at open circuit potential in 1 M Na<sub>2</sub>SO<sub>4</sub>; insets show zoomed Nyquist plots at high frequency region and the fitted equivalent circuit.

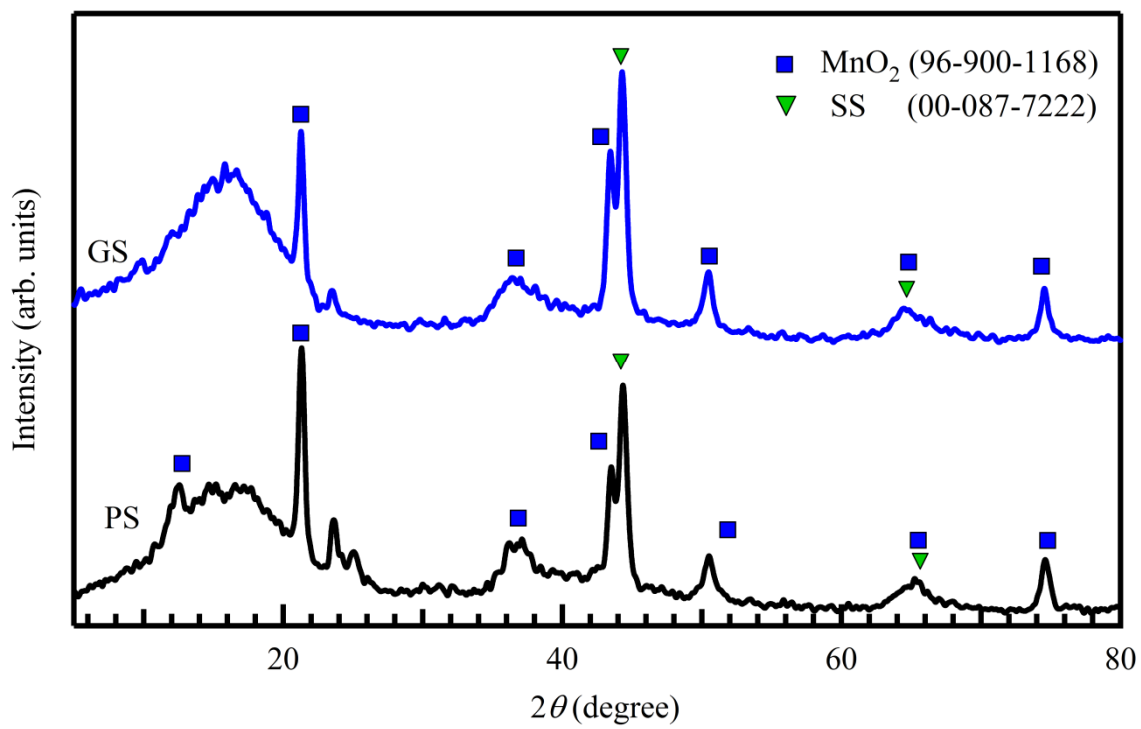


Figure 1

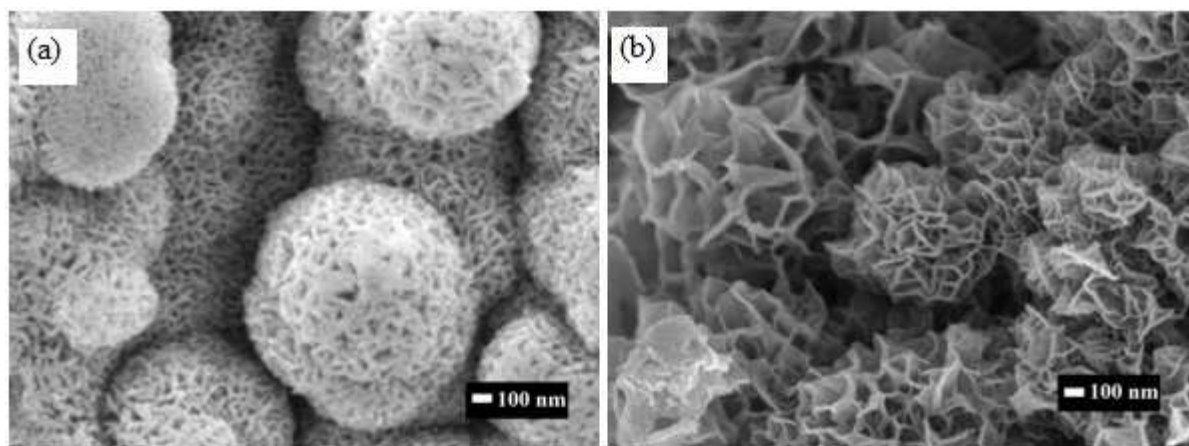
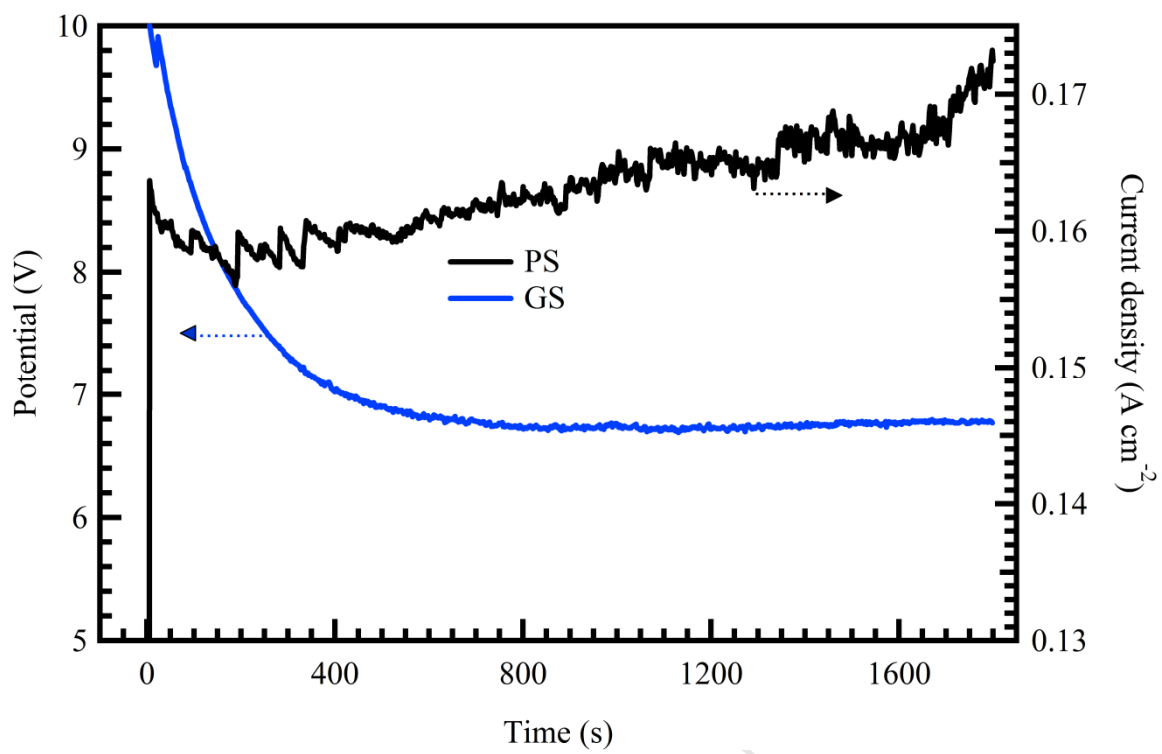


Figure 2

**Figure 3**

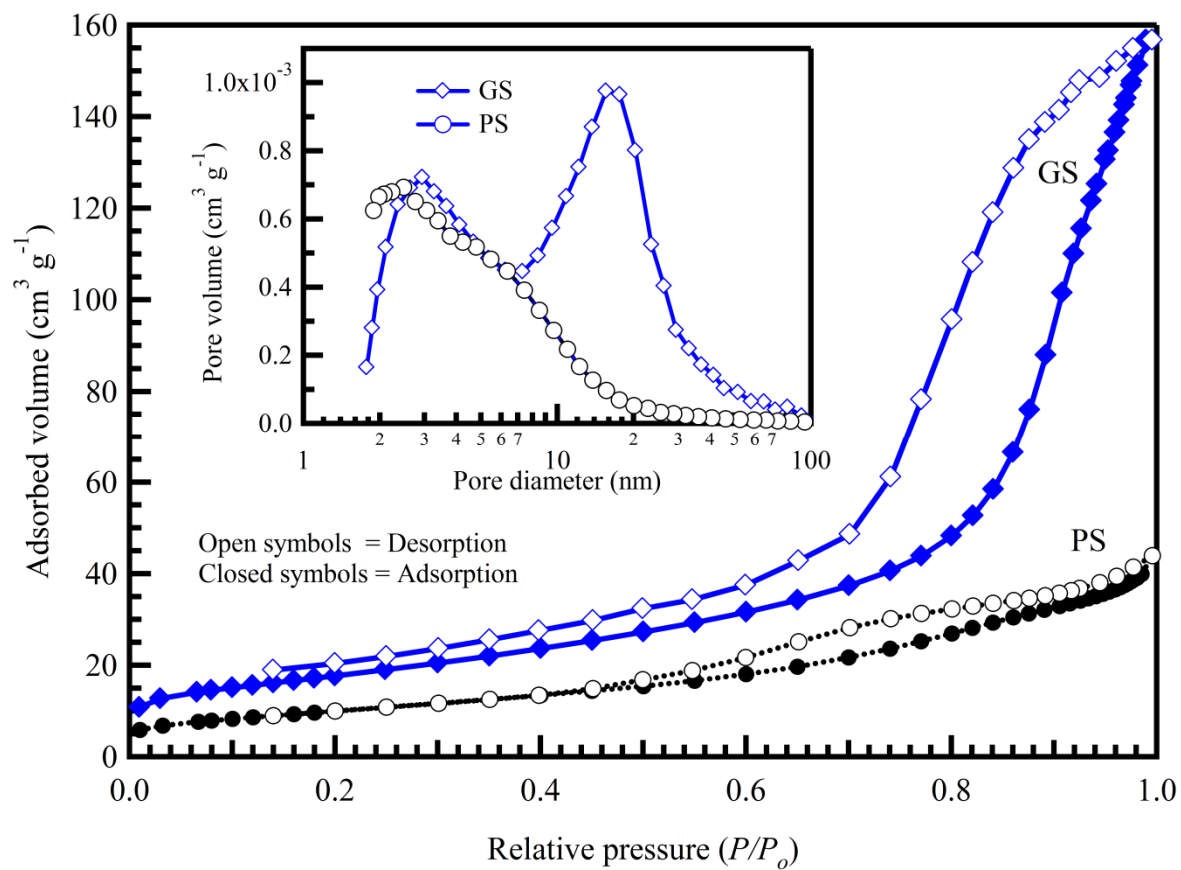


Figure 4

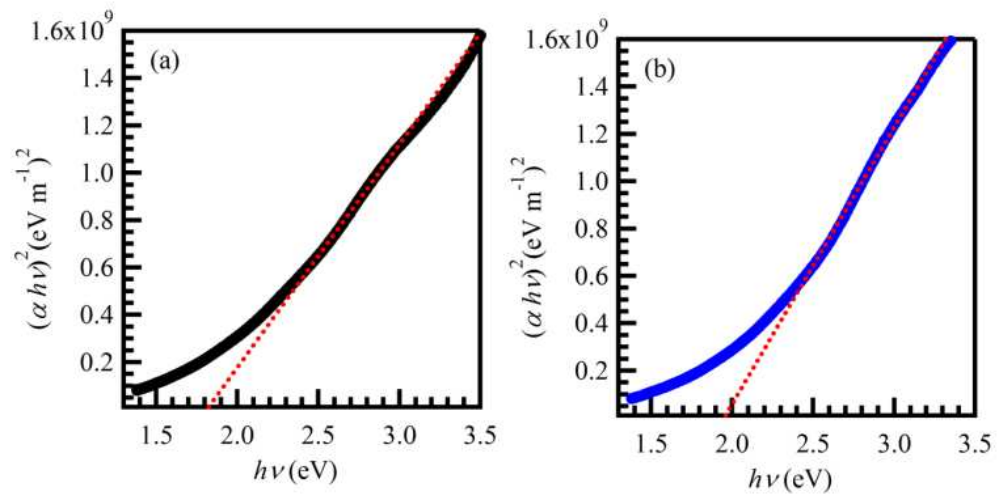


Figure 5

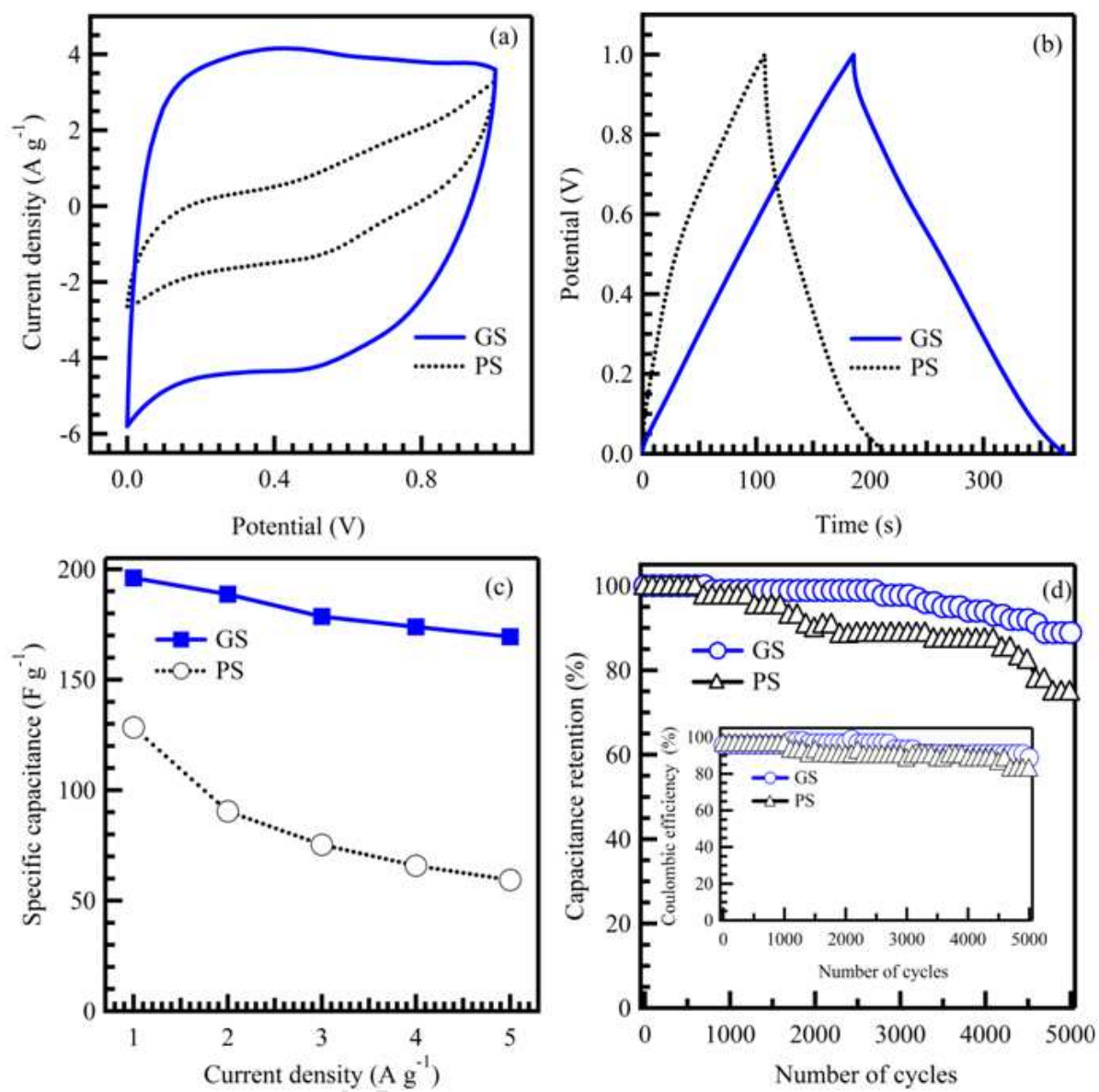


Figure 6

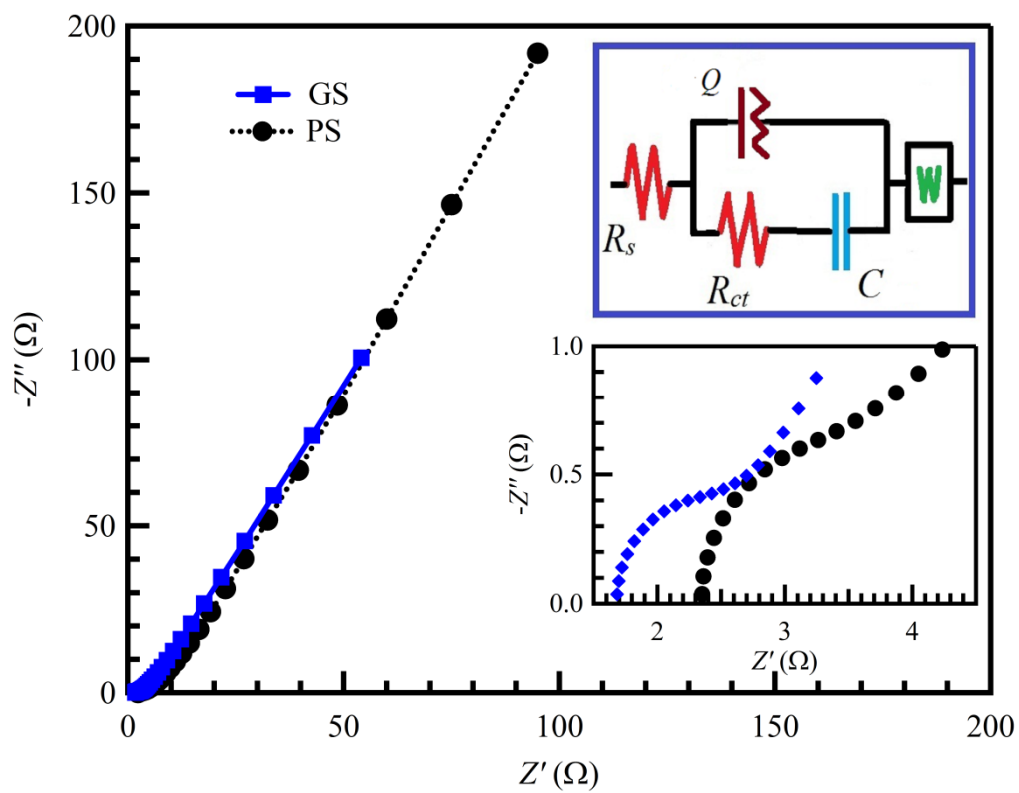


Figure 7

**Highlights**

- Galvanostatic deposition produced less compact MnO<sub>2</sub> nanostructures
- Galvanostatic deposition produced MnO<sub>2</sub> with wider band gap
- Galvanostatic deposition produced MnO<sub>2</sub> with high specific capacitance.
- Galvanostatic deposition is more suitable approach to produce MnO<sub>2</sub> for supercapacitor